

# Metabolic suppression identifies new antibacterial inhibitors under nutrient limitation

Soumaya Zlitni<sup>1,2</sup>, Lauren F Ferruccio<sup>2,3</sup> & Eric D Brown<sup>1,2\*</sup>

**Characterizing new drugs and chemical probes of biological systems is hindered by difficulties in identifying the mechanism of action (MOA) of biologically active molecules. Here we present a metabolite suppression approach to explore the MOA of antibacterial compounds under nutrient restriction. We assembled an array of metabolites that can be screened for suppressors of inhibitory molecules. Further, we identified inhibitors of *Escherichia coli* growth under nutrient limitation and charted their interactions with our metabolite array. This strategy led to the discovery and characterization of three new antibacterial compounds, MAC168425, MAC173979 and MAC13772. We showed that MAC168425 interferes with glycine metabolism, MAC173979 is a time-dependent inhibitor of *p*-aminobenzoic acid biosynthesis and MAC13772 inhibits biotin biosynthesis. We conclude that metabolite suppression profiling is an effective approach to focus MOA studies on compounds impairing metabolic capabilities. Such bioactives can serve as chemical probes of bacterial physiology and as leads for antibacterial drug development.**

The alarming spread of multidrug resistance is due in part to the fact that existing antibiotics target a very limited number of pathways, namely cell wall, DNA and protein biosynthesis<sup>1,2</sup>. There has been rising concern since the call to arms by the Infectious Diseases Society of America in 2004 about the general lack of innovation in the discovery of new antibacterials<sup>3</sup>, stressing the need to explore less conventional antimicrobial targets.

Since the turn of the 21st century, there have been remarkable developments in microbial genomics, target validation and screening technology, which have provided drug discoverers with many avenues to identify new antibacterials<sup>4</sup>. Moreover, given the challenges faced when attempting to convert inhibitors of recombinant targets into cell-active compounds, recent antibacterial drug discovery campaigns are shifting toward phenotype-based screening<sup>4</sup>. However, linking the phenotype (or phenotypes) caused by biologically active small molecules to specific mechanisms remains one of the biggest roadblocks in cell-based screening<sup>5</sup>.

In this respect, chemical genomic strategies have had considerable success in uncovering the MOA of biologically active molecules. Most important are efforts in the characterization of the MOA of small molecules by exploring their effects on genome-scale overexpression and deletion clone sets<sup>6–9</sup>. We have reported on manipulating gene dosage in *E. coli* as a systematic strategy toward identifying the cellular targets of new antibacterials and describing uncharted chemical genetic interactions for known antibiotics<sup>10,11</sup>.

In this work, we describe an approach that relies on using differential media screening as a strategy to explore the MOA of small molecules that inhibit bacterial growth under nutrient-limited conditions. When bacteria are grown in minimal medium, they undergo a substantial shift in their metabolic activities to support the requirements for *de novo* synthesis of amino acids, precursor molecules, vitamins and other cofactors<sup>12–14</sup>. Indeed, only 303 genes are essential for the growth of wild-type *E. coli* on rich medium, and some 119 genes are additionally required for growth on nutrient-limited medium<sup>15</sup>.

Small molecules that specifically target bacteria under nutrient limitation could serve as mechanistic probes to address biological

questions about nutritional stress responses. Moreover, some of these bioactives could be potential leads for the development of new antimicrobials. There have been many reports of impaired growth and attenuated virulence of various pathogens due to auxotrophy-generating gene deletions<sup>16–21</sup>. Combination therapy with sulfamethoxazole and trimethoprim, two inhibitors of folate biosynthesis, remains one of the most effective treatments for respiratory and urinary tract infections<sup>22</sup> and clearly validates targeting bacterial biosynthetic pathways in antibacterial therapy. Nevertheless, systematic searches for antibacterial chemicals have overwhelmingly emphasized rich nutrient conditions.

Metabolite supplementation has proven to be a formidable approach to understanding metabolic pathways in model microbes<sup>23</sup>. Herein we have exploited its power to investigate the MOA of biologically active small molecules. This strategy considerably narrows the number of potential targets to the benefit of mechanistic investigations. We have applied this approach to explore the antibacterial activity of both known antibiotics and new antibacterial compounds identified from a high-throughput screen of growth inhibition of *E. coli* under nutrient limitation. Through this approach, we generated characteristic fingerprints of small molecule–metabolite interactions that could inform on their biological activity. We report on the discovery of three new antibacterial compounds: MAC168425, which elicits its activity by interfering with glycine metabolism; MAC173979, a unique time-dependent inhibitor of *p*-aminobenzoic acid (PABA) biosynthesis; and MAC13772, an inhibitor of the enzyme BioA, the antepenultimate step in biotin biosynthesis. These inhibitors can serve both as specific chemical probes to study metabolic pathways in bacteria at a systems level and as potential leads for antibiotic drug discovery.

## RESULTS

### Screening for inhibitors in nutrient-deficient medium

A flow chart that outlines the different stages of our approach is shown in **Supplementary Results, Supplementary Figure 1**. Our work began with a high-throughput screen to identify compounds with growth inhibitory activity at a concentration of 10  $\mu$ M against

<sup>1</sup>Department of Biochemistry and Biomedical Sciences, McMaster University, Hamilton, Ontario, Canada. <sup>2</sup>Michael G. DeGroot Institute of Infectious Disease Research, McMaster University, Hamilton, Ontario, Canada. <sup>3</sup>Department of Chemistry and Chemical Biology, McMaster University, Hamilton, Ontario, Canada. \*e-mail: ebrown@mcmaster.ca

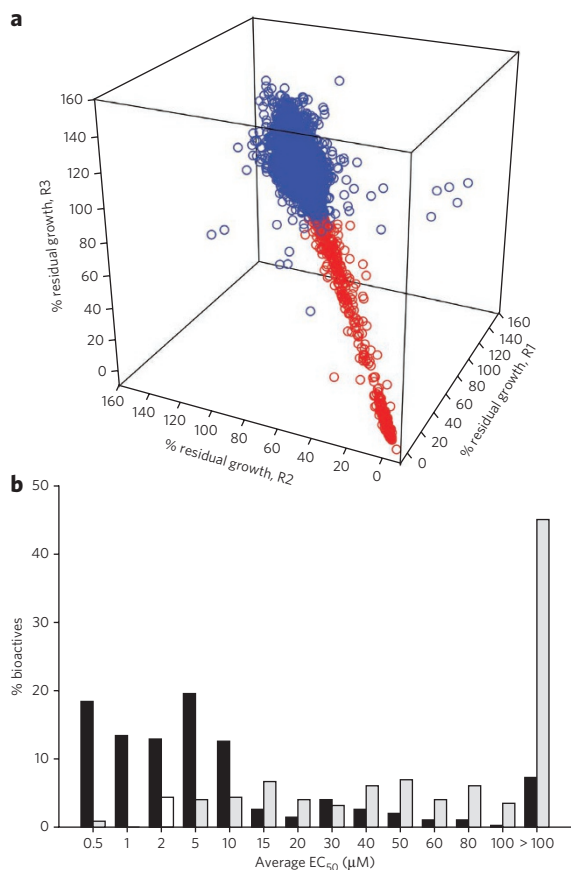


**Figure 1 | Primary small-molecule screen in minimal medium and  $EC_{50}$  evaluation of new bioactives.** (a) Three-dimensional replicate plot of the primary screen of ~30,000 small molecules against *E. coli* MG1655 grown in M9 minimal medium. Bacterial growth in the test wells is expressed as a percentage relative to the growth in the control wells (Supplementary Fig. 2). The percent residual growth of each replicate is plotted on each axis. Data points that fall on a slope of 1 are considered reproducible. Molecules that resulted in a residual growth below 80% for each replicate relative to the control wells were identified as biologically active against *E. coli* MG1655 in minimal medium (red circles) and were selected for further study (496 molecules). (b) Histogram of the average  $EC_{50}$  values obtained from the dose-response analysis of 340 new actives conducted in minimal (black bars) and supplemented minimal medium (gray bars).  $EC_{50}$  values were determined in duplicate in each medium condition (Online Methods and Supplementary Table 3).

*E. coli* MG1655 in nutrient-deficient medium from a library of ~30,000 molecules. This library includes structurally diverse small synthetic molecules, off-patent US Food and Drug Administration-approved and pharmacologically active molecules and purified natural products (Online Methods).

The primary screen was of high quality with respect to signal, noise and reproducibility, as shown in the control (Supplementary Fig. 2) and compound (Fig. 1a) data. The statistical parameter  $Z'$  describes the window between high and low controls and provides a measure to evaluate the quality of the screen<sup>24</sup>. For this screen, the average  $Z'$  value was 0.8. A cutoff of 80% residual growth was determined by calculating 3 s.d. from the high controls below 100% residual growth. This cutoff identified 496 actives that resulted in at least 20% growth inhibition relative to the high controls, corresponding to a hit rate of 1.7% (Fig. 1a). After eliminating known antibiotics, we arrived at a set of 340 new active compounds for further study. These were mainly synthetic small molecules constituting a set

of new chemical scaffolds with largely uncharacterized biological activity. In addition, there were a small number of natural products. Of the 340 compounds selected for follow up, there was a ~7% false positive rate.

### Differential media screening

To prioritize compounds that are specifically active under nutrient limitation, we conducted dose-response evaluations for all 340 compounds in nutrient-limited and in defined rich medium supplemented with a mix of amino acids, purines, pyrimidines and vitamins (Online Methods and Supplementary Table 2). These data were used to prioritize a subset of bioactives that perturbed bacterial physiology under nutrient-limited conditions. Supplementary Figure 3 shows examples of the assessment for two compounds. Notably, nearly a third of the 340 tested compounds exhibited a marked difference in potency against *E. coli* grown in the two different media. In fact, as many as 45% of the compounds showed no inhibition of bacterial growth within the tested concentration range in defined rich medium, in contrast to only 7% of the compounds with no activity against *E. coli* in minimal medium (Fig. 1b). Largely on the basis of potency and specificity to nutrient-limited conditions, we prioritized a total of 74 actives for follow-up analysis (half-maximum effective concentration ( $EC_{50}$ ) and minimum inhibitory concentration (MIC) values are listed in Supplementary Table 3).

### Metabolic suppression profiling

The strategy presented herein relies on perturbation using small molecules in a way that mimics genetic mutations in auxotrophic strains. To this end, we developed a secondary screen in which chemical complementation with metabolites was used as a rational approach to identify the potential cellular pathway (or pathways) targeted by the actives prioritized from the primary screen.

In this secondary screen, growth of *E. coli* in minimal medium containing an inhibitory concentration of each tested compound was examined against an array of single primary metabolites (amino acids, vitamins and nucleobases) and pools thereof (Supplementary Fig. 4).

The clustered heat map in Supplementary Figure 5 shows the metabolic suppression profile of the 74 prioritized actives and a set of known antibiotics with different MOA as controls to validate the approach. The profiles of a representative set of 24 inhibitors are shown in Figure 2.

The patterns of interaction between metabolites and inhibitors create unique metabolic suppression fingerprints that can be used to guide hypotheses regarding their MOA. The heat map in Supplementary Figure 5 is clustered on the basis of these metabolic suppression fingerprints so that compounds with similar profiles are grouped within the same cluster.

### Metabolic suppression profiles of known antibiotics

The metabolic suppression profiles of 22 known antibiotics of diverse MOA demonstrate the power of this approach (Supplementary Fig. 6). It is noteworthy that the activity of known antibiotics with mechanisms that do not directly involve primary metabolism, such as replication, transcription and translation inhibitors, was not altered in the presence of supplements. Inhibitors targeting biosynthetic capabilities, in contrast, displayed distinct metabolic suppression phenotypes mainly pertaining to their transport, MOA or both. Antimetabolites such as 5-fluorouracil and 6-azauracil, which inhibit different steps in pyrimidine nucleotide biosynthesis, were suppressed by uracil<sup>25,26</sup>. Growth inhibition by 6-aminonicotinamide was antagonized by niacin<sup>27</sup>; 6-thiopurine and 2,6-diaminopurine were antagonized by purine nucleobases. The actions of 3-thienylalanine, 5-methyltryptophan and *p*-fluorophenylalanine were reversed in the presence of aromatic amino acids<sup>28</sup>. The activity of the natural product 6-diazo-5-oxonorleucine, which targets

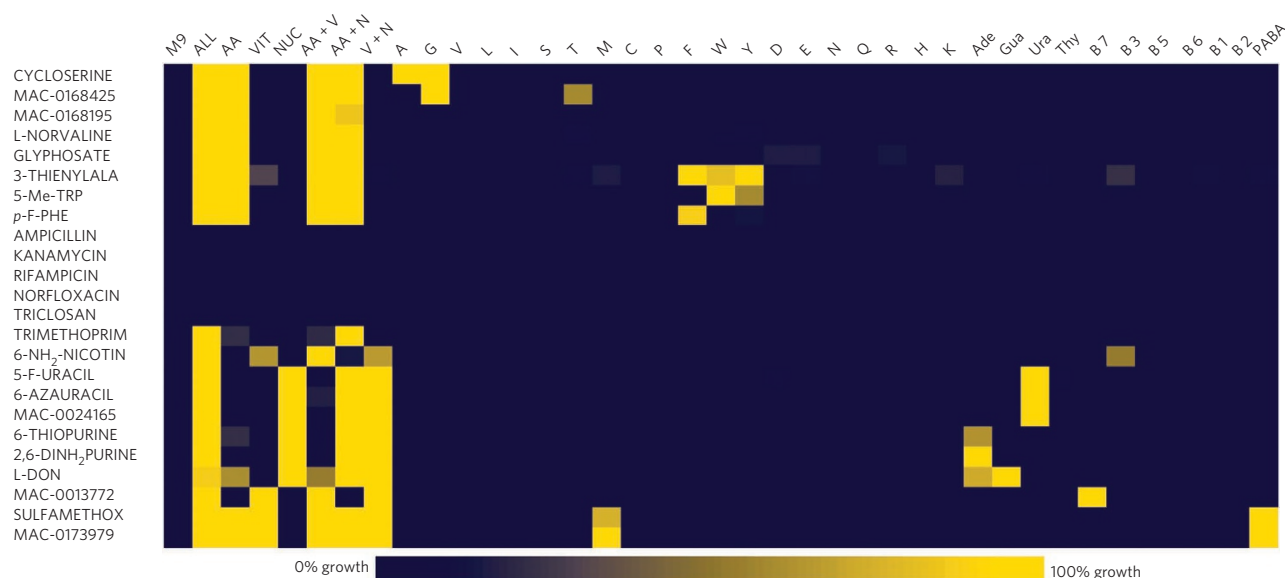


**Figure 2 | Metabolic suppression profiles of antibacterial inhibitors.** The metabolic suppression profiles of a representative set of 24 antibacterial inhibitors including 19 known antibiotics from **Supplementary Figure 5** are shown in this heat map. Growth of *E. coli* MG1655 is measured in the presence of each inhibitor with various primary metabolites or pools of metabolites in the metabolic suppression array ( $n = 2$  replicates) (Online Methods and **Supplementary Fig. 4**). Actives identified from the primary screen are designated by their MAC ID (details are in Online Methods), and the names of known actives are shown. Amino acids are referred to by their one-letter code, and B vitamins are referred to by their respective numbers. Ade, adenine; Gua, guanine; Ura, uracil; Thy, thymine; M9, no supplements; ALL, all supplements; AA, all amino acids; VIT, all vitamins; NUC, all nucleobases; 3-THIENYLALALA, L-3-thienylalanine; 5-Me-TRP, 5-methyltryptophan; *p*-F-PHE, *p*-fluorophenylalanine; 6-NH<sub>2</sub>NICOTIN, 6-aminonicotinamide; 5-F-URACIL, 5-fluorouracil; 2,6-DINH<sub>2</sub>-PUR, 2,6-diaminopurine; L-DON, 6-diazo-5-oxo-L-norleucine; SULFAMETHOX, sulfamethoxazole.

several glutamine-using enzymes in various metabolic pathways, was primarily suppressed by purine nucleobases<sup>29–31</sup>.

The cell wall inhibitor D-cycloserine was suppressed by either D,L-alanine or glycine. D-cycloserine, D-alanine and glycine use the same import mechanism, encoded by the transporter gene *cycA*<sup>32</sup>. Inside the cell, D-cycloserine is a competitive inhibitor of D-alanine D-alanine ligase (Ddl) in peptidoglycan biosynthesis<sup>33,34</sup> and of D-alanine racemase (DadX), which catalyzes the interconversion of D- and L-alanine<sup>35</sup>.

Inhibition by the antifolate antibiotic sulfamethoxazole was fully reversed by PABA and to an extent by methionine, a signature profile of inhibitors of PABA metabolism<sup>36</sup>. The enzymes PabA, PabB and PabC catalyze the biosynthesis of PABA from chorismate<sup>23</sup>. PABA is a precursor of folate coenzymes, which are involved in the transfer of one-carbon units in several pathways, including the biosynthesis of methionine, purines and pyrimidines<sup>37</sup> (**Supplementary Fig. 7**). Sulfamethoxazole and other sulfa drugs compete with PABA at the step of dihydropteroate synthesis (FolP) and enter the pathway as alternate substrates, ultimately creating dead-end products<sup>38</sup>. Addition of PABA outcompetes sulfamethoxazole, whereas methionine supplementation provides a major metabolite dependent on folate cofactors<sup>37</sup>.

Trimethoprim targets dihydrofolate reductase (FolA), which catalyzes the synthesis of tetrahydrofolate (**Supplementary Fig. 7**). As folate coenzymes are essential for the biosynthesis of glycine, methionine, pantothenate, formylated methionine and purine and pyrimidine nucleotides<sup>37</sup>, growth inhibition by trimethoprim could only be suppressed by providing a mixture of amino acids and nucleobases (**Supplementary Fig. 6**). The herbicide glyphosate inhibits 5-enol-pyruvylshikimate-3-phosphate synthase (AroA)<sup>39</sup>, which is involved in the biosynthesis of chorismate, a precursor of several metabolites, including the aromatic amino acids phenylalanine, tyrosine and tryptophan (**Supplementary Fig. 8a**)<sup>23</sup>. Accordingly, suppression of the activity of glyphosate could only be achieved by providing a mixture of amino acids (**Supplementary Fig. 8b**).

Metabolic suppression fingerprints, where growth inhibition could only be reversed by a pool of metabolites, were observed for about 20% of the profiled priority actives (**Supplementary Fig. 5**). This revealed the need to enrich the array with additional pools of metabolites that would, for example, accommodate blocks in early steps of branched metabolic pathways where more than one supplement would be required for suppression. In principle, the number of possible combinations of metabolites is very large. Nevertheless, a survey of primary metabolism in *E. coli* revealed a number of predated supplements, including pathway intermediates and metabolite pools. Thus, we created an expanded metabolic suppression array (**Fig. 3a**) where, for example, a mixture of aromatic amino acids fully reversed inhibition by glyphosate (**Supplementary Fig. 8c**). After profiling with the expanded metabolic suppression array, the activity of over half of the actives not suppressed by single supplements were further elaborated with suppression phenotypes using various pools of metabolites (**Fig. 3b**).

### MAC168425 interferes with glycine metabolism in *E. coli*

One of the clusters in the heat map in **Supplementary Figure 5** includes the profiles of seven priority actives that were strongly suppressed by the amino acid glycine (**Supplementary Fig. 9**). The activity of one of the molecules, MAC168425 (**1**), was strongly suppressed by glycine and to a lesser extent by L-threonine (**Supplementary Fig. 10**). In *E. coli*, glycine is primarily synthesized from serine in a one-step reaction catalyzed by serine-hydroxymethyl transferase (GlyA). This reaction is not only a source of glycine for protein synthesis but also the major source of one-carbon units needed for the synthesis of methionine, thymine, purines and pantothenate<sup>40</sup>. Threonine catabolism also contributes to the cellular pool of glycine. In the major pathway, threonine is converted to glycine through the action of threonine dehydrogenase (Tdh) and  $\alpha$ -amino- $\beta$ -ketobutyrate lyase (Kbl) (**Supplementary Fig. 11a**)<sup>40</sup>. In the minor pathway, low-specificity threonine aldolase degrades threonine to form glycine and acetaldehyde (**Supplementary Fig. 11b**)<sup>41</sup>.

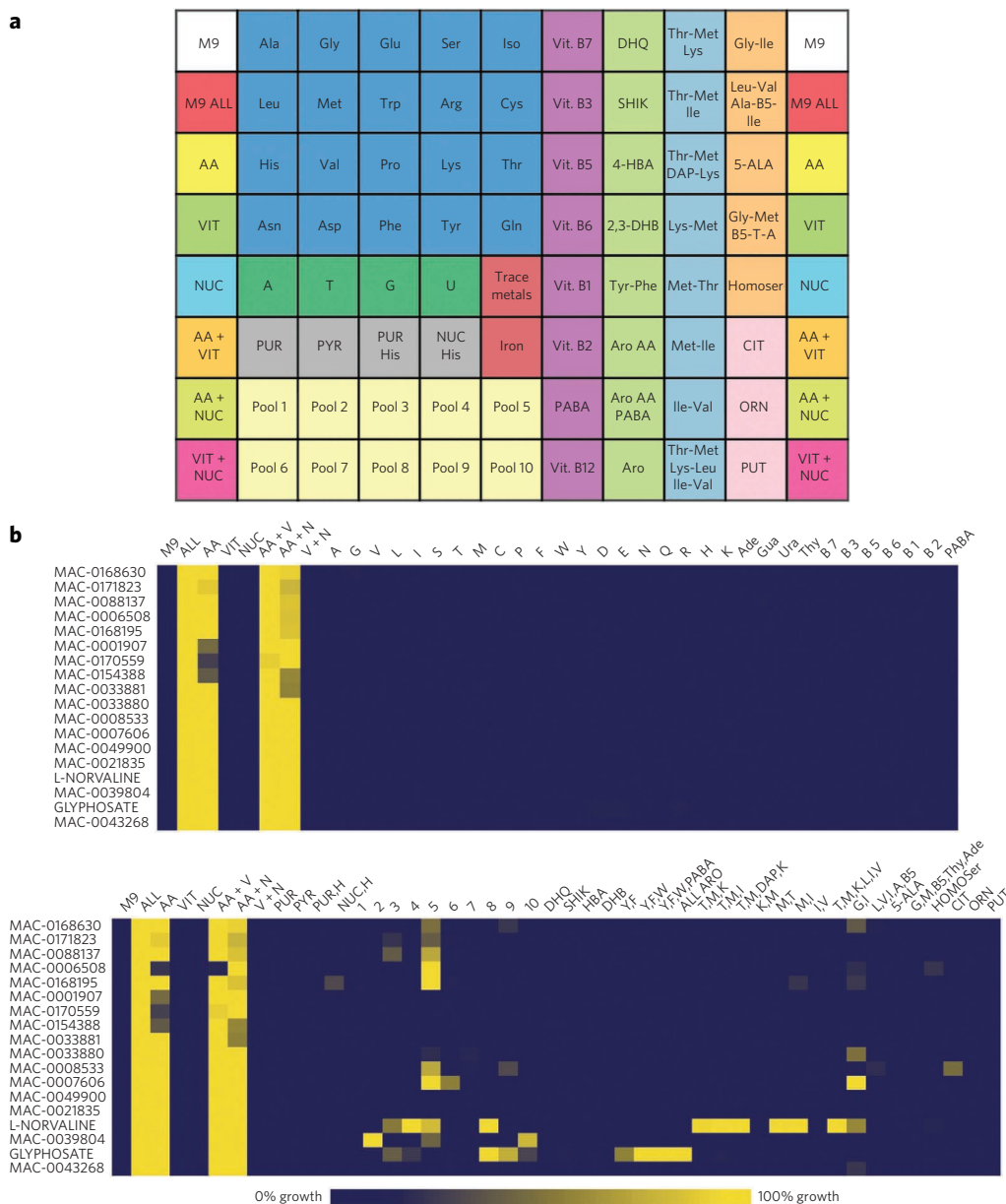


**Figure 3 | Pools of metabolites reveal more complex metabolic suppression patterns.** (a) The expanded metabolic suppression array. Amino acids are referred to by their three-letter codes, and nucleotides are listed by their one-letter code. M9, no supplements; ALL, all supplements; AA, all amino acids; VIT, all vitamins; NUC, all nucleobases; PUR, purine nucleobases; PYR, pyrimidine nucleobases; DHQ, 3-dehydroquinic acid; SHIK, shikimic acid; 4-HBA, 4-hydroxybenzoic acid; 2,3-DHB, 2,3-dihydroxybenzoic acid; Aro AA, aromatic amino acids (phenylalanine, tyrosine and tryptophan); Aro, aromatic amino acids, *p*-aminobenzoic acid, 4-hydroxybenzoic acid and 2,3-dihydroxybenzoic acid; DAP, diaminopimelic acid; 5-ALA, 5-aminolevulinic acid; Homoser, homoserine; CIT, citrulline; ORN, ornithine; PUT, putrescine. Further details are in Online Methods and **Supplementary Table 2**. (b) Top, cluster from the heat map in **Supplementary Figure 5** showing the metabolic suppression profiles of 18 inhibitors evaluated against the metabolic suppression array (**Supplementary Fig. 4**). The legend is the same as in **Figure 2**. Bottom, the metabolic suppression profile of the same inhibitors in the top panel after being evaluated against the expanded metabolic suppression array ( $n = 2$  replicates). The legend is the same as in **Figure 2** with the following additional abbreviations: PUR, purine nucleobases; PYR, pyrimidine nucleobases; DHQ, dihydroquinone; SHIK, shikimic acid; HBA, 4-hydroxybenzoic acid; DHB, 2, 3-dihydroxybenzoic acid; ALL ARO, aromatic amino acids, *p*-aminobenzoic acid, 4-hydroxybenzoic acid and 2,3-dihydroxybenzoic acid; DAP, diaminopimelic acid; 5-ALA, 5-aminolevulinic acid; HOMoser, homoserine; CIT, citrulline; ORN, ornithine; PUT, putrescine. Pools 1-10 are described in **Supplementary Table 2**.

Given that MAC168425 is strongly suppressed by glycine, partially suppressed by *L*-threonine and not suppressed by *L*-serine, we hypothesized that the connectivity between *L*-threonine and glycine metabolism underlies this metabolic suppression profile.

To test this, we tested suppression of the activity of MAC168425 by *L*-threonine in strains impaired in the threonine degradation pathways (**Supplementary Fig. 11c**). In the wild-type strain, MAC168425 has a four- to eightfold shift in its MIC in the presence of 40–640  $\mu\text{g ml}^{-1}$

of *L*-threonine. Within this range, *L*-threonine is generally less effective at suppressing growth inhibition by MAC168425 in a  $\Delta\text{tdh}$  mutant compared to a  $\Delta\text{ldaE}$  mutant. In a double deletion strain deficient in both the major and minor pathways ( $\Delta\text{ldaE } \Delta\text{tdh}$ ), the activity of MAC168425 is only suppressed at the highest concentrations of *L*-threonine tested (320–640  $\mu\text{g ml}^{-1}$ ), sustaining a two-fold shift in its MIC. In a triple deletion mutant strain ( $\Delta\text{ldaE } \Delta\text{tdh } \Delta\text{kbl}$ ), suppression of the activity of MAC168425 is completely lost.

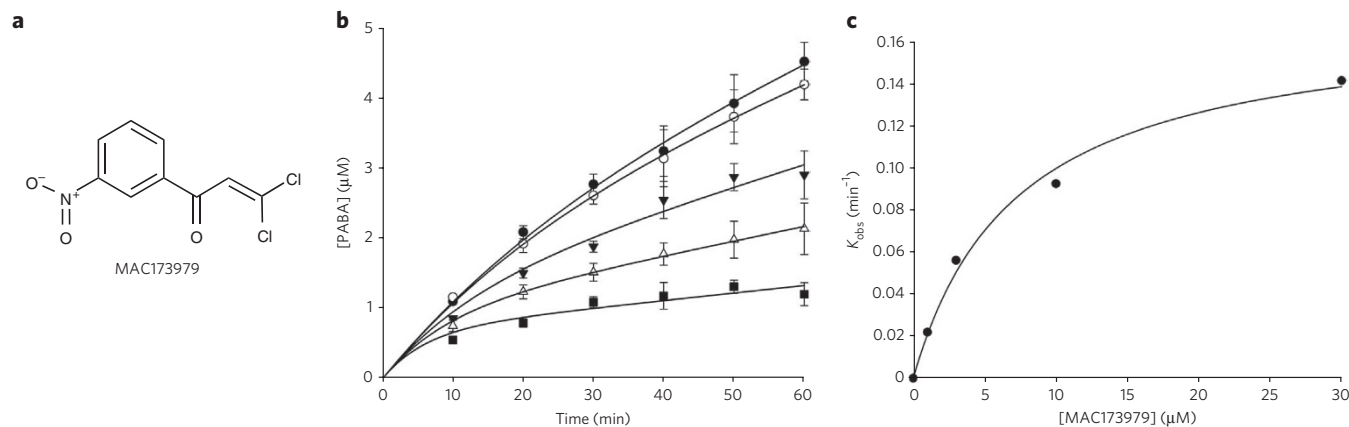


**Figure 4 | MAC173979 is an inhibitor of PABA biosynthesis in *E. coli*.** (a) Chemical structure of MAC173979. (b) Progress curves of the production of PABA in the presence of 0  $\mu\text{M}$  (closed circles), 1  $\mu\text{M}$  (open circles), 3  $\mu\text{M}$  (closed triangles), 10  $\mu\text{M}$  (open triangles) and 30  $\mu\text{M}$  (closed squares) of MAC173979. The assay was conducted by monitoring the conversion of chorismate to PABA in a one-pot enzyme assay of recombinant PabA–PabB–PabC complex using HPLC (Supplementary Fig. 15d). The data represent the averages of three replicates  $\pm$  s.d., and the progress curves are globally fitted to the rate equation of slow-binding inhibition<sup>42</sup> (Online Methods). (c) The plot of  $k_{\text{obs}}$  as a function of MAC173979 concentration fits a hyperbolic function suggesting a mechanism of inhibition where the initial EI complex is formed rapidly and then followed by a second slower conformational change to form the inactive EI\* complex (Supplementary Fig. 16). The data best fit the hyperbolic function defined by the equation  $k_{\text{obs}} = (k_5 [I]) / (K_i^{\text{app}} + [I])$ , which suggests that MAC173979 acts as an irreversible time-dependent inhibitor with an apparent  $K_i$  of  $7.3 \pm 1.3 \mu\text{M}$  (Online Methods).

It should be noted that the double and triple deletion mutants grow similarly to the wild-type parent strain and to the single deletion mutants (Supplementary Fig. 11d). These data strongly support the hypothesis that suppression of the lethality of MAC168425 by L-threonine is mediated through its conversion to glycine inside the cell and that the activity of this inhibitor most likely centers on reactions involving glycine production or utilization.

### MAC173979 inhibits PABA biosynthesis in *E. coli*

One of the major clusters in the heat map in Supplementary Figure 5 groups the metabolic suppression profiles of 15 priority actives with that of sulfamethoxazole (Supplementary Fig. 12). These compounds were suppressed when PABA, or to an extent methionine, were present in the growth medium, and all but one of these contain the *p*-aminobenzenesulfonamide moiety of sulfa drugs (Supplementary Fig. 13). The exception was the inhibitor MAC173979 (2), a dichloro-nitrophenyl propenone (Fig. 4a). Both PABA and methionine fully reversed the activity of MAC173979 (Supplementary Fig. 14). Indeed, the addition of PABA resulted in a 16-fold suppression of its MIC (Supplementary Fig. 15a) that was not observed with other metabolites derived from chorismate (Supplementary Fig. 15b). We hypothesized that MAC173979 could inhibit the folate pathway at the branch of PABA biosynthesis. PABA is synthesized from chorismate and L-glutamine in two steps catalyzed by three enzymes, PabA, PabB and PabC (Supplementary Fig. 15c)<sup>37</sup>. We reconstituted PABA synthesis with an HPLC-UV-based one-pot assay using recombinant PabA, PabB and PabC (Supplementary Fig. 15d). On addition of a mixture of enzymes to initiate the synthesis of PABA from chorismate and L-glutamine in the presence of different concentrations of MAC173979, the resulting reaction progress curves followed a curvilinear trend whereby each curve reached a slower steady-state rate after a fast initial velocity (Fig. 4b). This is characteristic of time-dependent enzyme inhibition<sup>42</sup>.

In principle, time-dependent enzyme inhibitors can follow either a simple reversible inhibition model or a two-step isomerization model (Supplementary Fig. 16). In the first mechanism, formation of the enzyme–inhibitor (EI) complex occurs in a single step on a slow timescale relative to the enzyme turnover. In the second, the EI complex undergoes a slower conformational change to form an inactive EI\* complex. When the dissociation constant of the EI\* complex is so low it approaches zero, the inhibitor is, for all practical

considerations, irreversible<sup>42,43</sup>. The relationship between the inhibitor concentration and  $k_{\text{obs}}$ , the apparent first order rate constant for the interconversion between the initial and steady-state rates, can help distinguish between the different mechanisms of inhibition. A plot of  $k_{\text{obs}}$  versus the inhibitor concentration  $[I]$  will be linear for the simple reversible model and hyperbolic for the slow isomerization model. The plot of the  $k_{\text{obs}}$  values versus MAC173979 concentration fits a hyperbolic function consistent with a mechanism of time-dependent inhibition that involves an isomerization of the EI complex (Fig. 4c). To discern whether there is an appreciable dissociation of the EI\* complex that contributes to the inhibition mechanism, we fit the data to two hyperbolic functions defined by the following equations:

$$k_{\text{obs}} = k_6 + \left[ \frac{k_5 [I]}{K_i^{\text{app}} + [I]} \right] \quad (1)$$

$$k_{\text{obs}} = \frac{k_5 [I]}{K_i^{\text{app}} + [I]} \quad (2)$$

Equation (2) provided the best fit for the experimental data, suggesting that MAC173979 acts as an irreversible time-dependent inhibitor of PABA synthesis with an apparent  $K_i$  of  $7.3 \pm 1.3 \mu\text{M}$  for all instances (mean  $\pm$  s.d.). Given that MAC173979 contains a Michael acceptor conjugated to highly electron-withdrawing groups (Fig. 4a), we reasoned that it could be susceptible to attack by an active site nucleophile with one of the two chlorines acting as a leaving group. However, when we determined the  $\text{IC}_{50}$  values of MAC173979 and an analog lacking the Michael acceptor, MAC173979-D (3), against the PabA–PabB–PabC system, we found them to be  $30 \pm 2 \mu\text{M}$  and  $60 \pm 7 \mu\text{M}$ , respectively (Supplementary Fig. 17a–c). Thus, although covalent chemistry cannot be ruled out at other potential sites of reactivity on this molecule, it remains a possibility that MAC173979 is a noncovalent, time-dependent inhibitor with a dissociation constant so low that it seems irreversible.

### MAC13772 inhibits biotin biosynthesis in *E. coli*

One compound in the heat map (Fig. 2), MAC13772 (4) (Fig. 5a), was uniquely suppressed by biotin (Supplementary Fig. 18). The late steps of biotin synthesis are catalyzed by the enzymes BioF, BioA, BioD and BioB (Supplementary Fig. 19)<sup>44</sup>. Recently, the roles

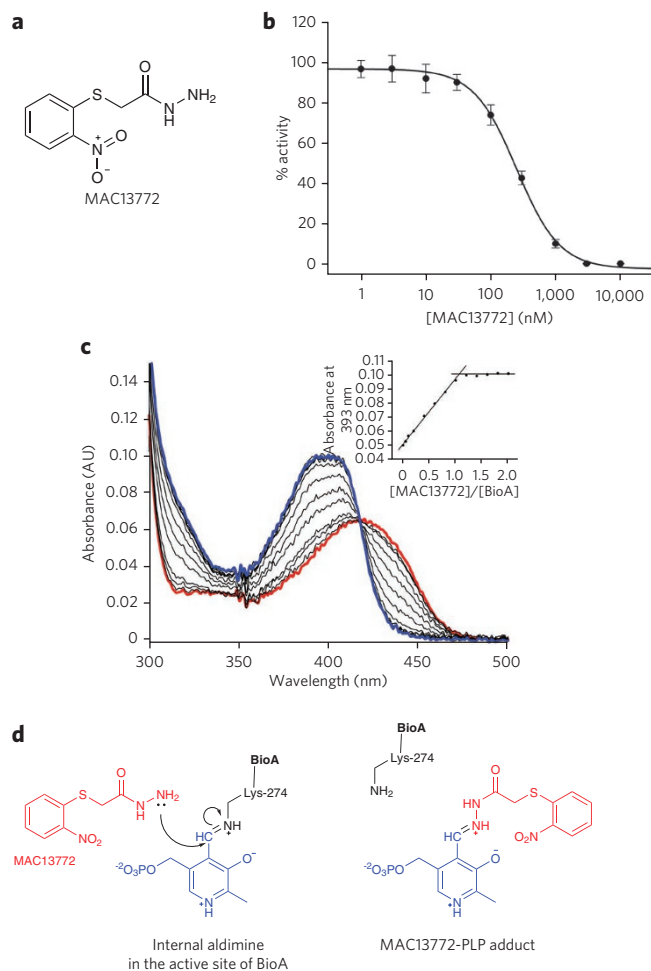


**Figure 5 | MAC13772 is an inhibitor of biotin biosynthesis in *E. coli*.**

(a) Chemical structure of MAC13772. (b) Dose-response curve of MAC13772 against recombinant BioA. The data represent the averages of six replicates  $\pm$  s.d., and the dose response curve was fitted to the four-parameter logistic nonlinear regression curve, yielding an  $IC_{50}$  value of  $250 \pm 28$  nM (Online Methods). (c) Spectral analysis of the BioA-MAC13772 interaction. BioA ( $5 \mu\text{M}$ ) was titrated with up to  $10 \mu\text{M}$  of MAC13772, and the UV-visible spectra of the mixture were recorded following each addition. The protein-ligand interaction is associated with a shift in the characteristic  $\lambda_{\text{max}}$  of PLP bound to the active site Lys274 from 420 nm, characteristic of the internal aldimine to 393 nm representing the newly formed PLP-inhibitor adduct. Red spectrum shows BioA before compound addition, and blue spectrum shows the BioA-MAC13772 mixture at the highest compound concentration tested. Inset, absorbance of the BioA-MAC13772 adduct at 393 nm versus the molar ratio of  $[\text{MAC13772}]/[\text{BioA}]$ . Note the absorbance plateauing at a molar ratio of -1, suggesting a 1:1 stoichiometric interaction between the inhibitor and the target. (d) Model for the BioA-MAC13772 interaction. The primary amine of the hydrazine group in MAC13772 displaces the Schiff base between Lys274 and PLP (internal aldimine) in the active site of BioA and reacts with the cofactor.

of BioC and BioH along with those of enzymes of fatty acid biosynthesis in providing the intermediate pimeloyl-ACP for the assembly of the biotin ring were elegantly demonstrated<sup>45</sup>.

Given that *E. coli* cells are permeable to the late intermediates in biotin biosynthesis, we tested the suppression of the inhibitory activity of MAC13772 in the presence of 7-keto-8-aminopelargonate (KAPA), 7,8-diaminopelargonate (DAPA) and dethiobiotin in comparison to the unsupplemented and biotin controls. Inhibition by

MAC13772 was fully reversed by DAPA, dethiobiotin and biotin, the products of the BioA, BioD and BioB reactions, respectively (Supplementary Table 4). In contrast, KAPA had no effect on MAC1372 activity. We thus reasoned that the step catalyzed by BioA was most likely the target of this inhibitor. BioA, also known as 7,8-diaminopelargonic acid synthase, is a pyridoxal phosphate (PLP)-containing transaminase that uses *S*-adenosylmethionine as an unusual amino donor to convert KAPA into DAPA<sup>46</sup>. We assayed the inhibitory activity of MAC13772 against recombinant *E. coli* BioA through a feeding assay of a *bioA* auxotroph (Online Methods). The dose-response curve in Figure 5b shows that MAC13772 is a potent inhibitor of BioA with an  $IC_{50}$  of  $\sim 250 \pm 28$  nM.

We hypothesized that inhibition of BioA by MAC13772 is most likely mediated through the interaction of the hydrazine moiety in the compound with PLP in the active site of the enzyme. To test this, we assessed the UV-visible spectra of BioA when titrated with the inhibitor. The interaction of MAC13772 with BioA is associated with a shift in the  $\lambda_{\text{max}}$  of the internal aldimine of the PLP-bound enzyme from 420 nm to 393 nm, representing the newly formed PLP-inhibitor adduct (Fig. 5c). The molar ratio plot of  $[\text{MAC13772}]/[\text{BioA}]$  (Fig. 5c) indicates that the interaction between the protein and the ligand is stoichiometric. A model of the BioA-MAC13772 interaction is shown in Figure 5d.

Having established the biochemical interaction of BioA with MAC13772, we were interested in exploring the structure-activity relationship (SAR) of this compound. We evaluated the antibacterial and biochemical activity of 24 analogs (Table 1 and Supplementary Table 5). We began by evaluating changes of substituents on the benzyl ring in the parent molecule and their position relative to the thioacetohydrazine chain (analog 5 through 13). All of the compounds in this category inhibited BioA, albeit with less potency compared to the parent compound MAC13772. However, the different modifications had a more substantial effect on their antibacterial activity against *E. coli*. Specifically, the position of the nitro group on the benzyl ring greatly influences biological activity, with the *ortho* position being highly favored (analog 5, 6 and 7). Alternatively, a chloro or a methyl substitution at the *ortho* position on the benzyl ring do not gravely alter antibacterial activity (analog 9 and 12). The requirement of the hydrazine moiety for the activity of MAC13772 was tested by either protecting it with an acetyl group or by modifying it (analog 14 through 18). Confirming our hypothesis, all of the analogs lacking the hydrazine group were completely inactive in both antibacterial and biochemical assays. Given this observation, we tested the activity of the side chain of varying lengths without the benzyl ring (analog 19 through 23). The varying hydrazine-containing side chains only showed slight to moderate *in vitro* inhibition of BioA and no considerable antibacterial activity. Notably, even in the case of the compounds 19 and 23, which had diminished antibacterial activity, growth inhibition was not suppressed in the presence of biotin. Replacing the benzyl ring in the parent compound with various rings was not tolerated, especially with respect to antibacterial activity (analog 24 through 28). This establishes the role of the benzyl ring for both the specificity and potency of MAC13772. Supplementary Figure 20 summarizes our findings from the SAR investigation.

## DISCUSSION

Characterizing the MOA of biologically active small molecules remains one of the biggest hurdles of whole cell-based screening in bacteria. In this work, we presented an approach that relies on metabolite suppression to explore the MOA of small molecules that target bacteria under nutrient-limited conditions. The metabolic suppression profiles of 22 known antibiotics revealed how this approach could provide information regarding the import, cellular target (or targets) and downstream effects of compounds that target bacterial physiology under nutrient restriction. Notably, we

Table 1 | SARs of MAC13772 and analogs

Compound	R <sup>1</sup>	R <sup>2</sup>	R <sup>3</sup>	R <sup>4</sup>	MIC (μg ml <sup>-1</sup> ) <sup>a</sup>		Percent inhibition <sup>b</sup>		
					-Bio	+Bio	1 μM	10 μM	
<b>MAC13772</b>	NHNH <sub>2</sub>	NO <sub>2</sub>	H	H	8	>256	100	100	
<b>Effect of substitution on benzene ring in Series a</b>									
<b>5</b>	NHNH <sub>2</sub>	H	NO <sub>2</sub>	H	256	>256	42	84	
<b>6</b>	NHNH <sub>2</sub>	H	H	NO <sub>2</sub>	64	>256	66	100	
<b>7</b>	NHNH <sub>2</sub>	H	H	H	64	>256	49	100	
<b>8</b>	NHNH <sub>2</sub>	F	H	H	32	>256	36	100	
<b>9</b>	NHNH <sub>2</sub>	Cl	H	H	16	>256	63	100	
<b>10</b>	NHNH <sub>2</sub>	OH	H	H	256	256	32	70	
<b>11</b>	NHNH <sub>2</sub>	NH <sub>2</sub>	H	H	256	>256	58	100	
<b>12</b>	NHNH <sub>2</sub>	CH <sub>3</sub>	H	H	16	>256	81	100	
<b>13</b>	NHNH <sub>2</sub>	OCH <sub>3</sub>	H	H	128	>256	65	100	
<b>Effect of changing hydrazine functionality on R<sup>1</sup> in Series a</b>									
<b>14</b>	NHNHAc	H	H	NO <sub>2</sub>	>256	>256	0	0	
<b>15</b>	CH <sub>2</sub> CH <sub>3</sub>	NO <sub>2</sub>	H	H	>256	>256	0	0	
<b>16</b>	NH <sub>2</sub>	NO <sub>2</sub>	H	H	>256	>256	0	0	
<b>17</b>	CH <sub>3</sub>	NO <sub>2</sub>	H	H	>256	>256	0	0	
<b>18</b>	OH	NO <sub>2</sub>	H	H	>256	>256	0	0	
<b>Activity of the side chain of the parent molecule in Series b</b>									
<b>19</b>	NH <sub>2</sub>	CH <sub>2</sub> SCH <sub>3</sub>			64	64	50	64	
<b>20</b>	NH <sub>2</sub>	CH <sub>2</sub> SH			256	256	20	34	
<b>21</b>	NH <sub>2</sub>	CH <sub>2</sub> CH <sub>2</sub> CH <sub>3</sub>			>256	>256	1	40	
<b>22</b>	NH <sub>2</sub>	CH <sub>2</sub> CH <sub>3</sub>			>256	>256	0	8	
<b>23</b>	NH <sub>2</sub>	CH <sub>3</sub>			128	128	7	19	
<b>Effect of different ring substituents in R<sup>2</sup> in Series b<sup>c</sup></b>									
<b>24</b>	NH <sub>2</sub>	Benzothiophene			>256	>256	15	69	
<b>25</b>	NH <sub>2</sub>	CH <sub>2</sub> SCH <sub>2</sub> Ph			64	>256	60	100	
<b>26</b>	NH <sub>2</sub>	CH <sub>2</sub> SNaph			>256	>256	71	100	
<b>27</b>	NH <sub>2</sub>	CH <sub>2</sub> SPyr			64	>256	32	77	
<b>28</b>	NH <sub>2</sub>	Nitrobenzyl			>256	>256	0	29	

<sup>a</sup>MIC values are determined against *E. coli* MG1655 in the absence and presence of 2 nM of biotin (Online methods). <sup>b</sup>The biochemical activity of analogs is determined against recombinant *E. coli* BioA through a feeding assay of a *bioA* auxotroph at 1 μM and 10 μM and is expressed as a percentage of the respective DMSO control (Online Methods). Ph, phenyl; Naph, naphthalenyl; Pyr, pyridine.

did not encounter suppression phenotypes that suggest off-target interactions. Furthermore, the consistency of the metabolic suppression profiles of known antibiotics with their well-characterized MOA suggests that this approach can provide a clear mechanistic fingerprint directly related to biological activity.

The metabolic suppression profile of MAC168425 illustrates the inter-relationship between glycine and threonine metabolism. Our work strongly suggests that its inhibitory activity is mediated through the biosynthesis or utilization of glycine. Our observation that L-threonine does not suppress the activity of MAC168425 in a *Δtdh* mutant as well as in a *ΔltaE* mutant is consistent with the fact that the Tdh-Kbl-mediated threonine catabolic pathway has a more important role in replenishing the cellular pool of glycine<sup>40</sup>. The need for a triple deletion mutant (*ΔltaE Δtdh Δkbl*) to fully abolish antagonism by threonine may be due to its being non-specifically oxidized to α-amino-β-ketobutyrate at high concentrations in the *ΔltaE Δtdh* mutant, which would allow glycine formation to

proceed through the major pathway. Processes involving glycine production and utilization are central to the biosynthesis of several essential cellular metabolites<sup>40</sup>. MAC168425 can provide a useful chemical probe to explore the interconnectivity of metabolic pathways centered on the transfer of one-carbon units.

The MOA of MAC173979 was of great interest to us because it displayed a characteristic fingerprint of inhibitors of PABA and folate metabolism but represented a previously unexplored chemical scaffold. Indeed, we have shown that MAC173979 is a time-dependent inhibitor of PABA synthesis in *E. coli* with a demonstrably slow off rate. In this respect, the effectively irreversible inhibition by this compound should resist competition from the buildup of substrate arising from upstream reactions. Notably, an analog of MAC173979 lacking the Michael acceptor had a comparable activity to the parent molecule, suggesting a MOA other than Michael addition. To our knowledge, MAC173979 represents the first PABA biosynthesis inhibitor with activity against Gram-negative bacteria.

MAC13772 provides an example of a potent inhibitor that targets vitamin metabolism. Biotin biosynthesis is a promising target for antimicrobial development<sup>47</sup> given that it is required by all forms of life but can only be synthesized by microorganisms and plants<sup>47,48</sup>. Furthermore, amounts of biotin in human serum are too low to provide adequate rescue to a pathogen impaired in biotin synthesis<sup>49</sup>. Our SAR investigation of 24 analogs of MAC13772 revealed the absolute requirement of the hydrazine group for activity. Hydrazine-containing molecules have found success in treating a variety of diseases (examples are in ref. 50). Many enzymes involved in biosynthetic pathways in *E. coli* are PLP-containing enzymes, so we found the strict dependence of MAC13772 activity on biotin restriction particularly intriguing. In this respect, the specificity and potency of the inhibitor seems to highly depend on the presence of the benzene ring and the nature of any substituents on it. This suggests a potentially important role for the ring in the interaction with BioA.

Small molecules that target metabolic pathways in bacteria growing under nutrient limitation allows for the investigation of bacterial physiology under conditions far from the standard laboratory culturing environment. This increases the number of potential targets that can be explored for antimicrobial drug development. Exploiting the power of metabolic complementation can markedly speed up the characterization of the MOA of small molecules of interest. Indeed, inhibitors of bacterial biosynthetic capabilities could provide a much needed addition to the dwindling repertoire of effective antibiotics.

Received 23 May 2013; accepted 29 August 2013;  
published online 13 October 2013

## METHODS

Methods and any associated references are available in the [online version of the paper](#).

## References

- Brown, E.D. Is the GAIN Act a turning point in new antibiotic discovery? *Can. J. Microbiol.* **59**, 153–156 (2013).
- Haselbeck, R. *et al.* Comprehensive essential gene identification as a platform for novel anti-infective drug discovery. *Curr. Pharm. Des.* **8**, 1155–1172 (2002).
- Boucher, H. *et al.* 10 × 20 Progress—development of new drugs active against gram-negative bacilli: an update from the Infectious Diseases Society of America. *Clin. Infect. Dis.* **56**, 1685–1694 (2013).
- Payne, D.J., Gwynn, M.N., Holmes, D.J. & Pompliano, D.L. Drugs for bad bugs: confronting the challenges of antibacterial discovery. *Nat. Rev. Drug Discov.* **6**, 29–40 (2007).
- Burdine, L. & Kodadek, T. Target identification in chemical genetics: the (often) missing link. *Chem. Biol.* **11**, 593–597 (2004).
- Parsons, A.B. *et al.* Integration of chemical-genetic and genetic interaction data links bioactive compounds to cellular target pathways. *Nat. Biotechnol.* **22**, 62–69 (2004).
- Giaever, G. *et al.* Chemogenomic profiling: identifying the functional interactions of small molecules in yeast. *Proc. Natl. Acad. Sci. USA* **101**, 793–798 (2004).
- Hoon, S. *et al.* An integrated platform of genomic assays reveals small-molecule bioactivities. *Nat. Chem. Biol.* **4**, 498–506 (2008); erratum **4**, 632 (2008).
- Lum, P.Y. *et al.* Discovering modes of action for therapeutic compounds using a genome-wide screen of yeast heterozygotes. *Cell* **116**, 121–137 (2004).
- Li, X. *et al.* Multicopy suppressors for novel antibacterial compounds reveal targets and drug efflux susceptibility. *Chem. Biol.* **11**, 1423–1430 (2004).
- Pathania, R. *et al.* Chemical genomics in *Escherichia coli* identifies an inhibitor of bacterial lipoprotein targeting. *Nat. Chem. Biol.* **5**, 849–856 (2009).
- Hua, Q., Yang, C., Oshima, T., Mori, H. & Shimizu, K. Analysis of gene expression in *Escherichia coli* in response to changes of growth-limiting nutrient in chemostat cultures. *Appl. Environ. Microbiol.* **70**, 2354–2366 (2004).
- Tao, H., Bausch, C., Richmond, C., Blattner, F.R. & Conway, T. Functional genomics: expression analysis of *Escherichia coli* growing on minimal and rich media. *J. Bacteriol.* **181**, 6425–6440 (1999).
- Zaslaver, A. *et al.* A comprehensive library of fluorescent transcriptional reporters for *Escherichia coli*. *Nat. Methods* **3**, 623–628 (2006).
- Baba, T. *et al.* Construction of *Escherichia coli* K-12 in-frame, single-gene knockout mutants: the Keio collection. *Mol. Syst. Biol.* **2**, 2006.0008 (2006).
- Chamberlain, L.M., Strugnell, R., Dougan, G., Hormaeche, C.E. & Demarco de Hormaeche, R. *Neisseria gonorrhoeae* strain MS11 harbouring a mutation in gene *aroA* is attenuated and immunogenic. *Microb. Pathog.* **15**, 51–63 (1993).
- Cuccui, J. *et al.* Development of signature-tagged mutagenesis in *Burkholderia pseudomallei* to identify genes important in survival and pathogenesis. *Infect. Immun.* **75**, 1186–1195 (2007).
- Mei, J.M., Nourbakhsh, F., Ford, C. & Holden, D. Identification of *Staphylococcus aureus* virulence genes in a murine model of bacteraemia using signature-tagged mutagenesis. *Mol. Microbiol.* **26**, 399–407 (1997).
- Polissi, A. *et al.* Large-scale identification of virulence genes from *Streptococcus pneumoniae*. *Infect. Immun.* **66**, 5620–5629 (1998).
- Samant, S. *et al.* Nucleotide biosynthesis is critical for growth of bacteria in human blood. *PLoS Pathog.* **4**, e37 (2008).
- Cersini, A., Salvia, A.M. & Bernardini, M.L. Intracellular multiplication and virulence of *Shigella flexneri* auxotrophic mutants. *Infect. Immun.* **66**, 549–557 (1998).
- Ho, J.M. & Juurlink, D. Considerations when prescribing trimethoprim-sulfamethoxazole. *CMAJ* **183**, 1851–1858 (2011).
- Pittard, J. & Yang, J. in *Escherichia coli and Salmonella: Cellular and Molecular Biology* (eds. Böck, A. *et al.*) (ASM Press, Washington, D.C., 2008).
- Zhang, J.H., Chung, T.D. & Oldenburg, K.R. A simple statistical parameter for use in evaluation and validation of high throughput screening assays. *J. Biomol. Screen.* **4**, 67–73 (1999).
- Longley, D.B., Harkin, D.P. & Johnston, P.G. 5-fluorouracil: mechanisms of action and clinical strategies. *Nat. Rev. Cancer* **3**, 330–338 (2003).
- Handschumacher, R.E. Orotidylic acid decarboxylase: inhibition studies with azauridine 5'-phosphate. *J. Biol. Chem.* **235**, 2917–2919 (1960).
- Cobb, J.R., Percy, S. & Gholson, R. Metabolism of 6-aminonicotinic acid in *Escherichia coli*. *J. Bacteriol.* **131**, 789–794 (1977).
- Richmond, M.H. The effect of amino acid analogues on growth and protein synthesis in microorganisms. *Bacteriol. Rev.* **26**, 398–420 (1962).
- Eidinoff, M.L., Knoll, J.E., Marano, B. & Cheong, L. Pyrimidine studies I. Effect of DON (6-diazo-5-oxo-L-norleucine) on incorporation of precursors into nucleic acid pyrimidines. *Cancer Res.* **18**, 105–109 (1958).
- Levenberg, B., Melnick, I. & Buchanan, J. Biosynthesis of the purines. XV. The effect of aza-L-serine and 6-diazo-5-oxo-L-norleucine on inosinic acid biosynthesis *de novo*. *J. Biol. Chem.* **225**, 163–176 (1957).
- Ahluwalia, G.S., Grem, J., Hao, Z. & Cooney, D. Metabolism and action of amino acid analog anti-cancer agents. *Pharmacol. Ther.* **46**, 243–271 (1990).
- Wargel, R.J., Shadur, C.A. & Neuhaus, F.C. Mechanism of d-cycloserine action: transport systems for D-alanine, D-cycloserine, L-alanine, and glycine. *J. Bacteriol.* **103**, 778–788 (1970).
- Zawadzke, L.E., Bugg, T.D. & Walsh, C.T. Existence of two D-alanine: D-alanine ligases in *Escherichia coli*: cloning and sequencing of the *ddlA* gene and purification and characterization of the DdlA and DdlB enzymes. *Biochemistry* **30**, 1673–1682 (1991).
- Neuhaus, F.C. & Lynch, J.L. The enzymatic synthesis of D-alanyl-D-alanine. 3. on the inhibition of D-alanyl-D-alanine synthetase by the antibiotic D-cycloserine. *Biochemistry* **3**, 471–480 (1964).
- Strominger, J.L., Ito, E. & Threnn, R.H. Competitive inhibition of enzymatic reactions by oxamycin. *J. Am. Chem. Soc.* **82**, 998–999 (1960).
- Stokstad, E.L. & Jukes, T.H. Sulfonamides and folic acid antagonists: a historical review. *J. Nutr.* **117**, 1335–1341 (1987).
- Green, J.M., Nichols, B.P. & Matthews, R.G. in *Escherichia coli and Salmonella: Cellular and Molecular Biology* (eds. Neidhardt, F.C. *et al.*) 665–673 (ASM Press, Washington, D.C., 1996).
- Walsh, C. *Antibiotics: Actions, Origins, Resistance* (ASM Press, Washington, D.C., 2003).
- Fischer, R.S., Berry, A., Gaines, C.G. & Jensen, R.A. Comparative action of glyphosate as a trigger of energy drain in eubacteria. *J. Bacteriol.* **168**, 1147–1154 (1986).
- Stauffer, G.V. in *Escherichia coli and Salmonella: Cellular and Molecular Biology* (eds. Böck, A. *et al.*) (ASM Press, Washington, D.C., 2004).
- Morris, J.G. Utilization of L-threonine by a pseudomonad: a catabolic role for L-threonine aldolase. *Biochem. J.* **115**, 603–605 (1969).
- Morrison, J.F. & Walsh, C.T. The behavior and significance of slow-binding enzyme inhibitors. *Adv. Enzymol.* **61**, 201–301 (1988).
- Copeland, R.A. *Enzymes: a Practical Introduction to Structure, Mechanism, and Data Analysis* (Wiley, New York, 2004).
- Cronan, J.E. in *Escherichia coli and Salmonella: Cellular and Molecular Biology* (eds. Böck, A. *et al.*) (ASM Press, Washington, D.C., 2008).



45. Lin, S., Hanson, R.E. & Cronan, J.E. Biotin synthesis begins by hijacking the fatty acid synthetic pathway. *Nat. Chem. Biol.* **6**, 682–688 (2010).
46. Stoner, G.L. & Eisenberg, M.A. Biosynthesis of 7,8-diaminopelargonic acid from 7-keto-8-aminopelargonic acid and S-adenosyl-L-methionine. The kinetics of the reaction. *J. Biol. Chem.* **250**, 4037–4043 (1975).
47. Shapiro, S. Speculative strategies for new antibacterials: all roads should not lead to Rome. *J. Antibiot. (Tokyo)* **66**, 371–386 (2013).
48. Schneider, G. & Lindqvist, Y. Structural enzymology of biotin biosynthesis. *FEBS Lett.* **495**, 7–11 (2001).
49. Woong Park, S. *et al.* Evaluating the sensitivity of *Mycobacterium tuberculosis* to biotin deprivation using regulated gene expression. *PLoS Pathog.* **7**, e1002264 (2011).
50. Lightcap, E.S. & Silverman, R. Slow-binding inhibition of  $\gamma$ -aminobutyric acid aminotransferase by hydrazine analogues. *J. Med. Chem.* **39**, 686–694 (1996).

## Acknowledgments

We thank B. Wanner of Purdue University and H. Mori of the Nara Institute for providing the Keio library clones used in these studies, F. Nizam for developing and assisting in using the in-house web-based unweighted pair group method with arithmetic mean (UPGMA)-based cluster analysis tool, M. Keramane for NMR

characterization of analogs used in this study and A. Capretta for inspiring discussions. We also thank J. Blanchard and C. Murphy for technical support during the primary screen. This work was supported by an operating grant from the Canadian Institutes of Health Research (MOP-81330) and by a Canada Research Chair award to E.D.B. S.Z. was supported by the Vanier Canada Graduate Scholarship.

## Author contributions

S.Z. designed and performed all experiments and co-wrote the manuscript. L.F.F. purified recombinant BioA and optimized cell-based and biochemical assays for the study of MAC13772 under the guidance of S.Z. E.D.B. conceived of and oversaw the project and co-wrote the manuscript.

## Competing financial interests

The authors declare no competing financial interests.

## Additional information

Supplementary information and chemical compound information is available in the [online version of the paper](#). Reprints and permissions information is available online at <http://www.nature.com/reprints/index.html>. Correspondence and requests for materials should be addressed to E.D.B.

## ONLINE METHODS

**Reagents.** Antibiotics were added to the medium as needed with final concentrations as follows: 100 µg/ml ampicillin, 20 µg/ml chloramphenicol and 50 µg/ml kanamycin. For the primary screen, the library compounds were prepared to a final concentration of 250 µM in 25% DMSO. For follow-up analysis, all compounds were solubilized in DMSO.

The library of ~30,000 small molecules was purchased from Maybridge Ltd., Cornwall, UK; ChemBridge Corp., San Diego, CA, USA; Prestwick Chemical, Plymouth Meeting, PA, USA; BIOMOL International, L.P., Plymouth Meeting, PA, USA; Sigma-Aldrich Canada Ltd., Oakville, ON, Canada and MicroSource Discovery Systems Inc., Gaylordsville, CT, USA. All of the library compounds are referred to by their respective MAC identification numbers. These are unique identifiers assigned by the McMaster High-throughput screening facility. The main compounds used in this study (MAC168425, MAC173979, MAC173979-D and MAC13772 and analogs 5 through 24) were purchased from their respective suppliers (listed in **Supplementary Tables 3 and 5**) and characterized by <sup>1</sup>H NMR, <sup>13</sup>C NMR and HR-MS (the chemical characterization data is in the **Supplementary Note**). KAPA was supplied from Santa Cruz Biotechnology, and DAPA was from Caymen Chemicals. All of the other chemicals and reagents were purchased from Sigma (Oakville, ON).

**Bacterial strains and culture conditions.** *E. coli* K-12 strains MG1655 and BW25113 were grown at 37 °C with aeration at 250 r.p.m. in liquid M9 minimal salts medium<sup>51</sup> with 0.4% glucose as a carbon source and 20 mM ammonium chloride as a nitrogen source. For all of the cell-based assays, the bacterial culture was prepared as follows: a single colony of *E. coli* was grown overnight in M9 minimal medium in a 37 °C incubator shaking at 250 r.p.m. The saturated overnight culture was diluted 1/50 in fresh M9 minimal medium and was grown in a 37 °C incubator with shaking at 250 r.p.m. until it reached an OD<sub>600</sub> of ~0.4–0.5. The subculture was then diluted 10<sup>3</sup>- and 10<sup>4</sup>-fold into fresh medium (minimal or supplemented, respectively) and set up to a final volume of 200 µl in clear flat-bottom 96-well plates.

**Primary screen in minimal medium.** The bacterial culture was prepared as described above. The clear flat-bottom 96-well assay plates were set up with the library compounds in triplicate to a final concentration of 10 µM and with high and low controls of 0.2% DMSO and 10 µg/ml of norfloxacin, respectively. Controls constituted 20% of each assay plate. All of the liquid handling was carried out using the Biomek FX liquid handler (Beckman Coulter Inc., Fullerton, CA). The mid-log subculture was then diluted 10<sup>3</sup>-fold into fresh M9 minimal medium and was set up in the assay plates using the µFill Microplate Dispenser (Biotek, Winooski, VT) to a final volume of 200 µl per well. Upon mixing of the bacterial culture with the screening compounds, the OD<sub>600</sub> of the plates was read using the Envision (PerkinElmer, Waltham, MA). The background reading was done to account for any interference due to low compound solubility in the growth medium or due to colored compounds. The plates were then incubated in a 37 °C stationary incubator for 12 h before measuring their OD<sub>600</sub>. A summary of the small-molecule screening data is in **Supplementary Table 1**.

**Analysis of the primary screen data.** The triplicate measurements were analyzed independently. Bacterial growth (*G*) was first calculated as follows:

$$G = OD_{600(t=16)} - OD_{600(t=0)}$$

where OD<sub>600(t=0)</sub> and OD<sub>600(t=16)</sub> correspond to absorbance of the samples before and after incubation of the assay plates, respectively. Converting bacterial growth (*G*) to % residual growth (%*G*) is calculated as follows:

$$\%G = \left( \frac{G_s - \mu_-}{\mu_+ - \mu_-} \right) \times 100$$

where *G<sub>s</sub>* is the bacterial growth in the presence of the tested compound, and *μ<sub>-</sub>* and *μ<sub>+</sub>* are the averages of the high and low controls, respectively. For hit selection, the statistical cutoff for the primary screen was 80% residual growth (3 s.d. below the high controls (100% residual growth)). Hence, compounds for which each of the triplicate measurements inhibited growth by at least 20% relative to the high controls was scored as a hit (an active) in the primary screen.

**Dose-response determination of priority actives.** The 11-point dose-response determinations were carried out in duplicate in two types of media: M9 minimal

medium and the same medium supplemented with amino acids, vitamins and nucleobases (recipe is in **Supplementary Table 2**). The bacterial culture was prepared as described above. The subculture was then diluted 10<sup>3</sup>- and 10<sup>4</sup>-fold into fresh M9 minimal medium and supplemented M9 minimal medium, respectively, and set up to a final volume of 200 µl in clear flat-bottom 96-well plates containing half-log serial dilutions of each tested compound (1 nM–80 µM) as well as high and low controls (0.2% DMSO and 10 µg/ml of norfloxacin, respectively). Upon mixing of the bacterial culture with the compounds, the OD<sub>600</sub> of the plates was read using the Envision (PerkinElmer, Waltham, MA) to account for background absorbance. The plates were then incubated in a 37 °C stationary incubator for 16 h before measuring their OD<sub>600</sub>.

**Analysis of dose-response determinations.** For each type of media, the duplicate EC<sub>50</sub> measurements were analyzed independently. Percent residual growth (%*G*) was calculated as described above.

%*G* was plotted against compound concentration on a semi-logarithmic plot and fit to the background corrected equation to determine EC<sub>50</sub>

$$\%G = \frac{\text{Range}}{1 + \left( \frac{[I]}{EC_{50}} \right)^S}$$

where 'range' is the difference between the maximum and minimum asymptotes of the curves at 0 and infinity [*I*], respectively; [*I*] is the concentration of the tested compound (µM); *S* is the slope (or Hill) factor; and EC<sub>50</sub> is the compound concentration that inhibits growth by 50%.

**Determinations of MIC.** Determinations of MIC were made for the compounds prioritized for follow-up studies. All of these compounds were reordered from suppliers. The MIC values were determined in liquid M9 minimal medium and minimal medium supplemented with amino acids, vitamins and nucleobases (medium composition is in **Supplementary Table 2**). The bacterial culture was prepared as described above. The diluted subculture in M9 minimal or supplemented minimal medium was then set up to a final volume of 200 µl in clear flat-bottom 96-well plates containing twofold serial dilutions of each tested compound (0.25–250 µg/ml). After mixing of the bacterial culture with the compounds, the OD<sub>600</sub> of the plates was read using the Envision (PerkinElmer, Waltham, MA) to account for background absorbance. The plates were then incubated in a 37 °C stationary incubator for 16 h before measuring their OD<sub>600</sub>. The MIC was defined as the lowest concentration of antibiotic that inhibits visible growth.

**Metabolic suppression profiling.** The metabolic suppression array was prepared in the format shown in **Figure 3a** and in **Supplementary Figure 4** as a 20× stock plate (concentrations are listed in **Supplementary Table 2**) to be used for metabolic suppression profiling. The bacterial culture was prepared as described above. The subculture was then diluted 10<sup>3</sup>-fold into fresh M9 minimal medium and set up to a final volume of 200 µl in clear flat-bottom 96-well plates containing 4× the MIC of each active and a 1/20 dilution of the metabolic suppression array stock plate. After mixing, the OD<sub>600</sub> of the plates was read using the Envision (PerkinElmer, Waltham, MA) to account for background absorbance. The arrays were then incubated at 37 °C for 16 h and their absorbance measured at 600 nm.

**Analysis of metabolic suppression profiles.** For each well in the metabolic suppression experiments, bacterial growth (*G*) was calculated as follows:

$$G = OD_{600(t=16)} - OD_{600(t=0)}$$

where OD<sub>600(t=0)</sub> and OD<sub>600(t=16)</sub> correspond to absorbance of the plates before and after incubation, respectively. % residual growth (%*G*) was calculated as follows:

$$\%G = \left( \frac{G_s - G_{M9}}{G_{M9ALL} - G_{M9}} \right) \times 100$$

where *G<sub>s</sub>* is the bacterial growth in the presence of the tested metabolite (or metabolites), and *G<sub>M9ALL</sub>* and *G<sub>M9</sub>* represent the bacterial growth in minimal and supplemented minimal medium, respectively.

The metabolic suppression profiles of the 93 actives shown in **Supplementary Figure 5** were hierarchically clustered using the Unweighted Pair Group Method with Arithmetic Mean (UPGMA) clustering method<sup>52,53</sup>, and the resulting tree was visualized using the open source software FigTree.

**Creation of double and triple deletion mutants in threonine catabolism.** Chromosomal DNA was prepared from single deletion mutants in *tdh*, *kbl* and *ltaE* obtained from the Keio library<sup>15</sup>. Primers designed to amplify 500 bp upstream and downstream the deletion region in each deletion strain were as follows: for the  $\Delta tdh$  region: 5'-ATATTATACCGGTACGCTTGG-3' and 5'-ATT TGCCCGTTGCCACTTCAATCC-3'; for the  $\Delta ltaE$  region: 5'-AGGCGACA GAGCCAGAACGT-3' and 5'-AGACCATATCGCGCATGACTTCG-3'; and for the  $\Delta kbl$  region: 5'-GAAAGAATTCTATAAATTAG-3' and 5'-CCCACC AGATCAAACGACAG-3'. To create a *tdh ltaE* double deletion mutant, the FRT-flanked kanamycin resistance cassette in  $\Delta tdh$  was eliminated using the FLP helper plasmid pCP20 as previously described<sup>54</sup>. About 2–4  $\mu$ g of purified PCR product from the  $\Delta ltaE$  region was transformed into the resistance marker-free  $\Delta tdh$  strain containing pKD46, and transformants were selected on LB agar medium with kanamycin (50  $\mu$ g/ml)<sup>15</sup>. The kanamycin resistance cassette was then eliminated from the *tdh ltaE* double deletion mutant by the same method described above. To create a *tdh ltaE kbl* triple deletion mutant, about 2–4  $\mu$ g of purified PCR product from the  $\Delta kbl$  region was transformed into the resistance marker-free  $\Delta tdh \Delta ltaE$  strain containing pKD46, and transformants were selected on LB agar medium with kanamycin (50  $\mu$ g/ml). All of the deletion mutants were verified by PCR to confirm that the genes of interest were deleted.

**Cloning, expression and purification of recombinant PabA, PabB and PabC.** To isolate PabA, PabB and PabC recombinant proteins, constructs were created to overexpress each protein with an N-terminal polyhistidine tag. Briefly, the genes encoding PabA, PabB and PabC were amplified from *E. coli* MG1655 genomic DNA using Phusion polymerase (Fermentas) using the following primers: for PabA: 5'-GGGGACAAGTTTGTACAAAAAAGCAG GCTTCGAAGGAGATACTAGCTAGATGATCCTGCTTATAGATA AC-3' and 5'-GGGGACCACTTTGTACAAGAAAGCTGGGTCTCAGCGAT GCAGGAAATTAGC-3'; for PabB: 5'-GGGGACAAGTTTGTACAAAAAAG CAGGCTTCGAAGGAGATACTAGCTAGATGAAGACGTTATCTCC CGCT-3' and 5'-GGGGACCACTTTGTACAAGAAAGCTG GGTCTTACT TCTCCAGTTGCTTCAG-3'; for PabC: 5'-GGGGACAAGTTTGTACAAAA AAGCAGGCTTCGAAGGAGATACTAGCTAGATGTTCTTAATTAACGG TCAT-3' and 5'-GGGGACCACTTTGTACAAGAAAGCTGGGTCTTAAT TCGGGCGCTCACAAAG-3'. The PCR products were purified and cloned into pDEST17 using the Gateway cloning and Expression Kit (Invitrogen, Canada), and the constructs were confirmed by DNA sequence analysis (MOBIX, McMaster University). Each construct was transformed into *E. coli* BL21AI electrocompetent cells before protein expression and purification. The following procedure was followed for the expression and purification of each of the three proteins. For protein expression, each clone was grown in 2 l of LB with ampicillin (100  $\mu$ g/ml) at 37 °C with shaking at 250 r.p.m. until the culture reached an OD<sub>600</sub> of 0.6. The culture was then induced with 0.2% l-arabinose and grown for an additional 3 h before harvesting by centrifugation at 10,000g. The cell pellets were resuspended and washed with a 0.85% saline solution, pelleted and stored at –20 °C. For protein purification, the cell pellets were thawed and resuspended in 25 mL of lysis buffer (50 mM Tris, pH 7.5, 500 mM NaCl, 15 mM imidazole, 2 mM BME, 0.5 mg DNase, 0.5 mg RNase, protease inhibitor cocktail (Roche)). Cells were lysed by passage through a cell disrupter with continuous flow at 30,000 psi and clarified by centrifugation at 40,000g for 1 h. The clarified lysate was purified by nickel-chelating chromatography using a 1-mL HiTrap affinity column (GE Healthcare, Mississauga, Canada). The column was washed with buffer A (50 mM Tris, pH 7.5, 500 mM NaCl, 15 mM imidazole, 2 mM BME) and eluted with a linear gradient of 15–300 mM of imidazole. Fractions were analyzed by SDS-PAGE, and those containing pure His-tagged protein were pooled and desalted through a HiPrep 26/10 desalting column (GE) against the final storage buffer (50 mM Tris, pH 7.5, 10% glycerol). The concentration of purified proteins was determined by the Bradford assay (Bio-Rad). About 20 mg were obtained for each of the three enzymes. Fractions rich in pure protein were stored in aliquots at –80 °C.

**Pab enzyme assays.** Enzyme assays were conducted in triplicate at room temperature with 25 nM of PabA and PabB, 50 nM of PabC, 50 mM Tris-HCl (pH 7.5), 20  $\mu$ M PLP, 1 mM l-glutamine, 40  $\mu$ M chorismate and the concentrations of MAC173979 indicated in **Figure 4b**. The inhibition assays were initiated by addition of a mixture of the three enzymes and quenched with an equal volume of freshly prepared 8 M urea. The reaction progress curves were

monitored every 10 min for 60 min and determined by a stopped HPLC assay that allowed for the quantification of the conversion of chorismate to PABA. The two analytes were separated on a C<sub>18</sub> reverse phase column (Nova-Pak C18, 4  $\mu$ m, 3.9  $\times$  150 mm, Waters) and eluted isocratically with 5% acetic acid in double distilled H<sub>2</sub>O<sup>55</sup>. The analytes were visualized by UV absorbance at 275 nm and identified by comparing their retention times and UV absorption spectra to authentic standards. The progress curves were plotted to the rate equation of slow-binding inhibition<sup>42,43</sup>

$$[\text{Product}] = v_s \times t + \frac{(v_0 - v_s)}{k_{\text{obs}}} \times (1 - e^{-k_{\text{obs}} \times t})$$

using Sigma Plot 12.0 (SPSS, Inc., Chicago, IL), where  $v_0$  and  $v_s$  are the initial and final steady-state reaction velocities, respectively;  $t$  is the time; and  $k_{\text{obs}}$  is the apparent first order rate constant for the interconversion between the initial and steady-state rates.

**Expression and purification of recombinant BioA.** To isolate recombinant BioA protein, the strain AG1-pCA24N-*bioA* (JW0757) from the ASKA library was used. The clone was grown in 2 l of LB with chloramphenicol (80  $\mu$ g/ml) at 37 °C, with shaking at 250 r.p.m. until the culture reached an OD<sub>600</sub> of 0.6. The culture was then induced with 0.1 mM IPTG and grown for an additional 3 h before harvesting by centrifugation at 10,000g. The cell pellet was resuspended and washed with a 0.85% saline solution, pelleted and stored at –20 °C. For protein purification, the cell pellet was thawed and resuspended in 25 mL of lysis buffer (50 mM HEPES, pH 8, 500 mM NaCl, 100  $\mu$ M PLP, 50 mM imidazole, 0.5 mg DNase, 0.5 mg RNase and protease inhibitor cocktail (Roche)). Cells were lysed by passage through a cell disrupter with continuous flow at 30,000 psi and clarified by centrifugation at 40,000g for 1 h. The clarified lysate was purified by nickel-chelating chromatography using a 1-mL HiTrap affinity column (GE Healthcare, Mississauga, Canada). The column was washed with buffer A (50 mM HEPES, pH 8, 500 mM NaCl, 100  $\mu$ M PLP, 50 mM imidazole) and eluted with a linear gradient of 50–400 mM of imidazole. Fractions were analyzed by SDS-PAGE, and those containing pure His-tagged protein were pooled and desalted through a HiPrep 26/10 desalting column (GE) against the final storage buffer (50 mM HEPES, pH 8, 10% glycerol). The concentration of purified proteins was determined by the Bradford assay (Bio-Rad). The BioA yield was about 30 mg from cell pellets from 2 l of culture. Fractions rich in pure protein were stored in aliquots at –80 °C.

**BioA assay.** For the determination of the IC<sub>50</sub> of MAC13772, the BioA enzyme assay was conducted in triplicate at room temperature with 100 nM of BioA, 100 mM HEPES buffer (pH 8.5), 15  $\mu$ M of KAPA, 1 mM of S-adenosylmethionine and 1–10,000 nM of MAC173979 (the half-log serial dilutions of inhibitor stocks were made in 25% DMSO to reduce the final DMSO concentration in the assay to 0.5%). The 100- $\mu$ L reactions were initiated by addition of the enzyme and quenched after 20 min with 10  $\mu$ L of 100% trichloroacetic acid. DAPA production was biologically determined on the basis of a strategy originally described for biotin<sup>56</sup>. The plates were prepared as previously described<sup>45</sup>. A 5-mL culture of *E. coli* BW25113  $\Delta bioA$  (from the Keio library) was grown overnight in M9 minimal medium supplemented with 2 nM biotin. Cells from the saturated culture were pelleted and washed in fresh minimal medium (without biotin) and pelleted again. The pellet was resuspended in 25 mL of fresh minimal medium (without biotin). The subculture was grown at 37 °C, 250 r.p.m. for 4–5 h to deplete biotin. Cells are then pelleted and washed again in 10 mL of minimal medium. Cells were mixed to a final OD<sub>600</sub> of 0.1 into 50 mL of M9 minimal agar (1.5%) containing 2,3,5-triphenyl tetrazolium chloride to a final concentration of 0.1% (w/v). The mixture (16 mL) was poured into single-well plates (Nunc OmniTray, 128 mm  $\times$  86 mm). To evaluate BioA activity, 10  $\mu$ L of each reaction was spotted on a 6-mm disc (BBL) placed on the agar plates. Plates were incubated for 24 h at 37 °C, and growth zones appeared as a deep pink formazan deposit. The plates were scanned using an Epson Perfection v750, and the radii of growth were measured using Fiji<sup>57</sup> with a scale of 22 pixels/mm. The amount of DAPA formed from the reactions was estimated on the basis of a DAPA standard curve (5–600 pmol) where growth was linear with the logarithmic amount of DAPA spotted. The DAPA standard curve was conducted with every experiment.

For each inhibitor concentration, the amount of DAPA formed (pmol) was expressed as a percentage of the DMSO control, and the dose-response curve

was plotted to the four parameter logistic nonlinear regression model

$$\%activity = \min + \frac{(\max - \min)}{1 + \left(\frac{[I]}{IC_{50}}\right)^{-Hill\ Slope}}$$

using Sigma Plot 12.0 (SPSS, Inc., Chicago, IL), where 'min' is the minimum asymptote at infinity [I], 'max' is the maximum asymptote in the absence of the inhibitor, [I] is the concentration of the tested compound (nM), Hill Slope is the slope (steepness) of the curve and  $IC_{50}$  is the compound concentration that inhibits enzyme activity by 50%.

For the evaluation of the activity of the different MAC13772 analogs, the reactions were set up in duplicate as described above in the presence of each inhibitor at 1  $\mu$ M and 10  $\mu$ M (at a final DMSO concentration of 0.25% and 2.5%, respectively). For each analog, the amount of DAPA formed was expressed as a percentage of the respective DMSO control (% activity) and the % inhibition was calculated as (100 – % activity).

**Spectral analysis of BioA-MAC13772 interaction.** A 1-mL mixture of 5  $\mu$ M of BioA in 50 mM of HEPES buffer (pH 7.5) was titrated with up to 10  $\mu$ M of MAC13772. The titration was monitored by measuring the UV-visible spectra

(from 300–500 nm) in a 1-mL quartz cuvette after each addition of the inhibitor using Varian Cary Bio 300 UV-visible spectrophotometer.

51. Sambrook, J. & Russell, D.W. *Molecular Cloning: A Laboratory Manual* (Cold Spring Harbor Laboratory Press, New York, 2001).
52. Sneath, P.H.A. & Sokal, R.R. *Numerical Taxonomy: The Principles and Practice of Numerical Classification* (W. H. Freeman, San Francisco, 1973).
53. Romesburg, C. *Cluster Analysis For Researchers* (Lulu Press, Morrisville, N.C., 2004).
54. Baba, T. & Mori, H. The construction of systematic in-frame, single-gene knockout mutant collection in *Escherichia coli* K-12. *Methods Mol. Biol.* **416**, 171–181 (2008).
55. Walsh, C.T., Erion, M., Walts, A., Delany, J. & Berchtold, G. Chorismate aminations: partial purification of *Escherichia coli* PABA synthase and mechanistic comparison with anthranilate synthase. *Biochemistry* **26**, 4734–4745 (1987).
56. Genghof, D.S., Partridge, C.W. & Carpenter, F.H. An agar plate assay for biotin. *Arch. Biochem.* **17**, 413–420 (1948).
57. Schindelin, J. *et al.* Fiji: an open-source platform for biological-image analysis. *Nat. Methods* **9**, 676–682 (2012).